

Characterization of a medium-sized washer-gun for an axisymmetric mirror

Hongshen Yi, Ming Liu, Peiyun Shi, Zhida Yang, Guanghui Zhu, Quanming Lu, and Xuan Sun

Citation: [Review of Scientific Instruments](#) **89**, 043503 (2018); doi: 10.1063/1.5013118

View online: <https://doi.org/10.1063/1.5013118>

View Table of Contents: <http://aip.scitation.org/toc/rsi/89/4>

Published by the [American Institute of Physics](#)

Articles you may be interested in

[Improving the viability and versatility of the \$E \times B\$ probe with an active cooling system](#)

[Review of Scientific Instruments](#) **89**, 043502 (2018); 10.1063/1.5004469

[Analysis of retarding field energy analyzer transmission by simulation of ion trajectories](#)

[Review of Scientific Instruments](#) **89**, 043501 (2018); 10.1063/1.5018269

[Field-reversed configuration formed by in-vessel \$\theta\$ -pinch in a tandem mirror device](#)

[Review of Scientific Instruments](#) **88**, 093505 (2017); 10.1063/1.5001313

[Metrological 2iOF fibre-optic system for position and displacement measurement with 31 pm resolution](#)

[Review of Scientific Instruments](#) **89**, 045001 (2018); 10.1063/1.5029563

[An integrated single- and two-photon non-diffracting light-sheet microscope](#)

[Review of Scientific Instruments](#) **89**, 043701 (2018); 10.1063/1.5020154

[Calibrated work function mapping by Kelvin probe force microscopy](#)

[Review of Scientific Instruments](#) **89**, 043702 (2018); 10.1063/1.5007619

PHYSICS TODAY

WHITEPAPERS

MANAGER'S GUIDE

Accelerate R&D with
Multiphysics Simulation

READ NOW

PRESENTED BY

 COMSOL

Characterization of a medium-sized washer-gun for an axisymmetric mirror

Hongshen Yi,¹ Ming Liu,¹ Peiyun Shi,¹ Zhida Yang,¹ Guanghui Zhu,¹ Quanming Lu,² and Xuan Sun^{1,2,a)}

¹Department of Modern Physics, University of Science and Technology of China, Hefei 230026, China

²CAS Key Laboratory of Geospace Environment, No. 96, JinZhai Road, Baohe District, Hefei, China

(Received 10 November 2017; accepted 14 March 2018; published online 3 April 2018)

A new medium-sized washer gun is developed for a plasma start-up in a fully axisymmetric mirror. The gun is positioned at the east end of the Keda Mirror with AXisymmetry facility and operated in the pulsed mode with an arc discharging time of 1.2 ms and a typical arc current of 8.5 kA with 1.5 kV discharge voltage. To optimize the operation, a systematic scan of the neutral pressure, the arc voltage, the bias voltage on a mesh grid 6 cm in front of the gun and an end electrode located on the west end of mirror, and the mirror ratio was performed. The streaming plasma was measured with triple probes in the three mirror cells and a diamagnetic loop in the central cell. Floating potential measurements suggest that the plasma could be divided into streaming and mirror-confined plasmas. The floating potential for the streaming plasma is negative, with an electric field pointing inwards. The mirror-confined plasma has a typical lifetime of 0.5 ms. *Published by AIP Publishing.* <https://doi.org/10.1063/1.5013118>

I. INTRODUCTION

The once-thriving tandem-mirror fusion research has been nearly stagnant for several decades. During this period, the axisymmetric tandem mirror has been proposed by several researchers,^{1–3} which was re-evaluated by Fowler *et al.*^{4,5} recently. In addition to the past lessons learned in plasma stabilization, their evaluation is also based on the newest breakthrough on heating electrons in the gas-dynamic trap (GDT) machine.⁶ The axisymmetric mirror configuration will be more engineering-friendly and economical to construct. The magnetohydrodynamic (MHD) instability plaguing the tandem mirror plasmas can be solved by introducing a kinetic stabilizer, instead of using the mini-B configuration, and the confinement can be improved by electron heating solely in the plug cells. Many scenarios in that paper remain to be tested.

Here, as a first step in studying these new ideas for axisymmetric mirrors, the behavior of the initial plasma generated by a new washer gun at one end of a fully axisymmetric mirror facility (KMAX, Keda Mirror with AXisymmetry) is reported. Washer guns have been employed to initiate the plasma in most mirror experiments because of efficiency and high output. For example, a washer-gun-generated plasma was serving as the ion source for the neutral beams of the fully axially symmetric ambipolar magnetic mirror trap (AMBAL-M) experiments,⁷ as well as a target plasma in the central cell.⁸ Extensive studies on plasma confinement and instability using gun-generated plasmas as a target plasma have been conducted on GDT.^{9–12} GAMMA 10 routinely uses radio frequency (RF) waves to generate, sustain, and heat the plasma; it has also used gun-produced plasma to study axial and radial confinement.^{13–17} More examples can be found in Phaedrus/Phaedrus-B^{18–20} and Tandem Mirror Experiment (TMX) and Upgrade (TMX-U)^{21,22} tandem mirrors.

In addition to the application as a plasma source, a streaming plasma can provide the conductivity between the electrode of the gun and the target plasma. Thus, it was also used for electrical bias experiments. For example, in the Madison Symmetric Torus (MST),^{23,24} a washer gun injecting plasma along the tangential direction of the torus yielded a significantly improved confinement by creating a radial electric shear. Another successful application in this regard was achieved in C-2,^{25–27} where the azimuthal velocity direction was changed by the radially inward electric field. And at the same time, the $E \times B$ shearing rate was significantly increased which improved stability.

Here, the new washer gun, which has a different size and geometry relative to previous guns, is a modified version of the miniature gun used in the MST device. Its purpose is to provide a denser plasma for ion cyclotron heating in the central cell as well as the control of radial electric fields.

II. KMAX DEVICE AND THE WASHER GUN

A. KMAX introduction

The KMAX is an axisymmetric mirror consisting of a central cell and two end cells. As shown in Fig. 1, the axial length of the KMAX device, without counting the plasma source or the other parts that are attached to the float endplate, is 9.6 m and the central cell length is 5.2 m. The inner diameters of the central chamber and the mirror throat are 1.2 m and 0.3 m, respectively, and the wall thickness is 10 mm. Three sets of turbo pump, one 1200 l/s in each end mirror cell and one 2000 l/s in the central cell, are used to pump the background pressure down to 6×10^{-7} Torr. Figure 2 depicts the plasma gun location with the extracting grid and a flat disk end electrode in a plot of the magnetic flux profile.

B. Design of the washer gun

A schematic of the medium-sized gun is shown in Fig. 3(a), and the electric field lines calculated using Comsol

^{a)} Author to whom correspondence should be addressed: xsun@ustc.edu.cn

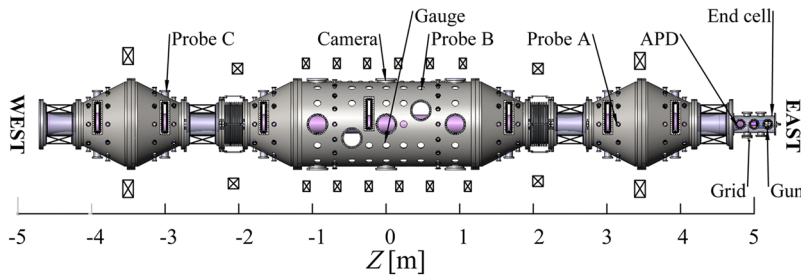


FIG. 1. Schematic of the KMAX device and the three Langmuir probe locations at the east, central, and west cells. The end cell is connected to the end of the east mirror throat, and the washer gun was placed at the end cell. There is a mesh grid 6 cm in front of the gun, the fast camera, and the fast ion gauge in the central cell.

is shown in Fig. 3(b). The diameter is 25 mm, the length is 67 mm, and the total volume is about $3.29 \times 10^{-5} \text{ m}^3$. The anode and cathode are molybdenum, and a stack of molybdenum washers, 2-mm thick with 25-mm inner diameters and 65-mm outer diameters, were placed in between to define the electric potential profile. The molybdenum washers are isolated from each other with boron nitride (BN) ceramic washers with 2-mm thicknesses and inner and outer diameters of 45 mm and 65 mm, respectively. The distance from the cathode to the anode is 50 mm. The entire structure is covered with BN ceramic to isolate it from the vacuum vessel.

The gun is operated in the pulsed mode. Two different gas puff valves have been tested: a SevenStar™ electromagnetic valve (model number: DJ2CVUG6) and a piezoelectric gas leak valve (PEV-1). The piezoelectric valve can be precisely controlled in time and gas flow, while the electromagnetic valve is vulnerable in the electromagnetic environment and is imprecise due to the jitter of its mechanical motion. However, it provides a much larger gas flow with a range of

50 standard liters per minute, whereas the piezoelectric ceramic valve has a maximum flow rate of 500 SCCM, producing a moderate plasma density. Thus, the EM valve is used, with a home-made power supply as in Ref. 28.

A molybdenum mesh grid is mounted 6 cm in front of the gun muzzle to extract the plasmas. The grid can be floated or biased relative to the gun anode or the end electrode at the other end of machine. In Secs. III B and III C below, data for different biasing are discussed.

Neutral diffusion is monitored by a nude fast ion gauge mounted flush with the wall at $z = 0 \text{ m}$. In Fig. 4 are pressure signals ranging over 0.05–0.4 MPa at the valve. The main purpose of the gauge is to provide an estimation of the neutral gas diffusion speed; therefore, it is not absolutely calibrated. There is a time delay caused by the 0.5 m path from the valve to the gun cathode, in addition to the distance from the gauge to the gun. For operation at 0.3 MPa, the arc trigger time is $t = 0 \text{ ms}$.

A type “B” pulse forming network (PFN)²⁹ with five sections was constructed in-house to provide a discharge current of 1.224 ms in duration. Parameters of the PFN elements are calculated according to $\tau = 2\sqrt{L_n C_n}$, $Z_n = \sqrt{L_n/C_n}$, $C_n = \tau/(2Z_n)$, $C = C_n/n$, $L_n = 1/2 \times \tau Z_n$, $L = L_n/n$ ($n = 1, 2, 3, \dots$), where n is the number of staves (PFN sections), τ is the PFN pulse duration, Z_n is the characteristic impedance, C_n is the total network capacitance, C is the capacitance per stave, L_n is the total network inductance, and L is the inductance per stave. Here, $L = 15 \mu\text{H}$ and $C = 1000 \mu\text{F}$, with a pulse duration

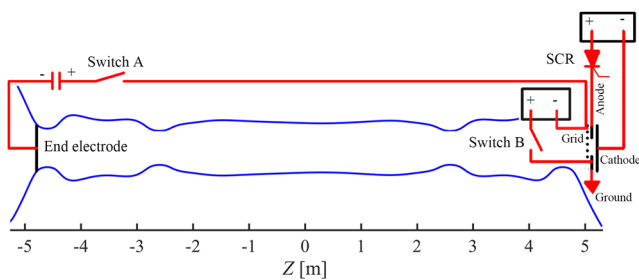


FIG. 2. Schematic of the gun plasma flux in KMAX, and a diagram of the washer gun circuit, mesh-grid bias, and end-electrode bias (gun and electrode are not to scale).

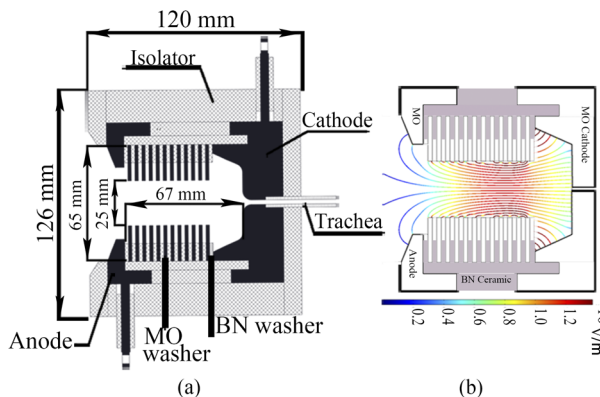


FIG. 3. (a) Schematic of the washer gun and (b) the simulation of the gun electric field.

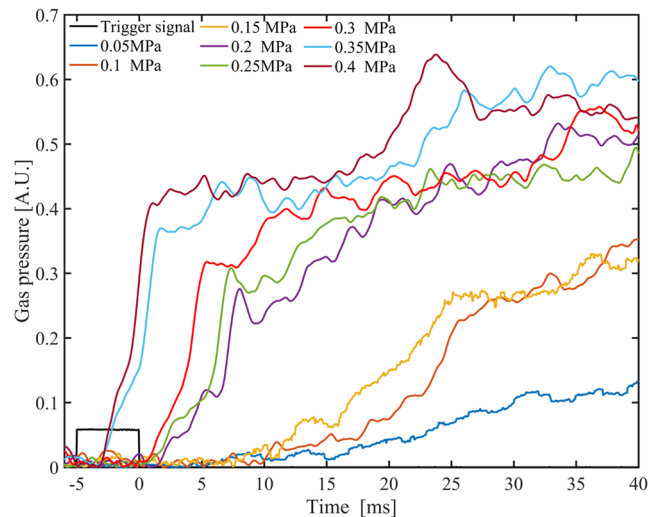


FIG. 4. Neutral gas injection signal at different pressures monitored by a fast gauge at $z = 0 \text{ m}$.

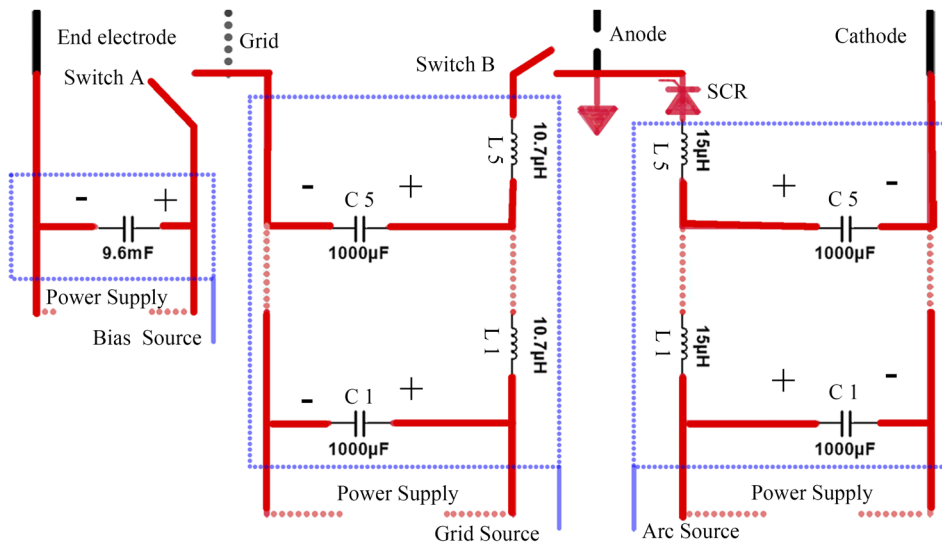


FIG. 5. Diagram of the circuit for the washer gun PFN, grid PFN, and end electrode.

of $\tau = 1.224$ ms. The circuit diagram is shown in Fig. 5. Thus, the stored energy for a 1.5-kV charge voltage on the PFN is 5.625 kJ.

C. Performance of the plasma gun

In our experiment, the working gas is hydrogen. A typical performance of the plasma gun is shown in Fig. 6. The arc current was measured by a LEM™ current transducer, module number LT 4000-S with a 100-kHz bandwidth, and a response time (90% of I_{max}) < 1 μ s. It is plotted as a red line, which agrees well with the simulations (black dashed line) using the Multisim software. The grid voltage, V_{ga} , was measured by a voltage divider with an AD215 isolation amplifier. The optical

emission was detected at $z = 4.9$ m in the nearby end cell by an Avalanche Photodiode (APD), model number APD410AM with bandwidth 10 MHz and wavelength range from 400 nm to 1000 nm. The noise on the APD signal is very similar to that reported previously by Osher³⁰ and McCarrick *et al.*,³¹ which is believed to play an important part in ion heating via wave-particle interactions. For this measurement, the PFN was charged to 1.5 kV and the grid voltage was biased at -0.5 kV. The grid power supply is also a five-section PFN source with $L = 10.7$ μ H and $C = 1000$ μ F.

After $t = 1.45$ ms, the gun power supply is switched off and the discharge current is essentially zero. However, from the APD light signal near the grid, the plasma lasts an additional ~ 1 ms, as shown in Fig. 6(d), which could be due to the grid bias. The collected grid current I_g , shown in Fig. 6(b), is reversed, which is caused by circuit oscillations in the grid power supply, which has a different switch than that used for the power supply of the gun arc. The voltage on the grid [Fig. 6(c)] also changes to ~ 100 V.

The charging voltage V_s of the PFN power supply was then varied, with the grid voltage set to -0.5 kV and 0.3-MPa of injected gas. Both the discharge current I_d and the arc voltage V_a vs. V_s are plotted in Fig. 7, and the values are then averaged over $t = 0.5$ ms to $t = 1.0$ ms. Note that there is a considerable voltage drop in the circuit from the PFN power

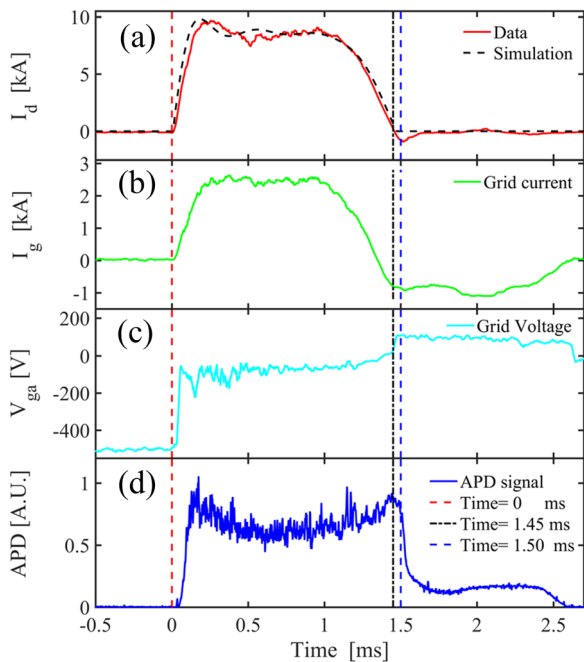


FIG. 6. (a) Measured arc current and simulated current using Multisim, (b) measured grid current, and (c) the voltage on the grid relative to the anode of the gun. (d) APD signal measured at $z = 4.9$ m. For this measurement, $V_s = 1.5$ kV, $V_g = -0.5$ kV, and gas pressure is 0.3 MPa.

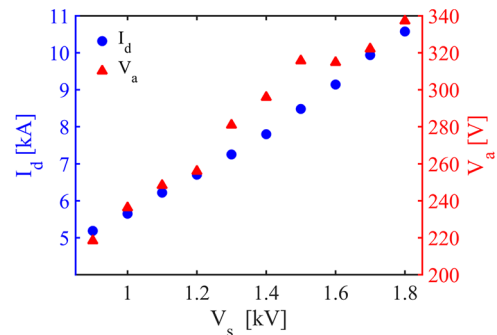


FIG. 7. The arc voltage V_a and current I_d vs. PFN voltage V_s . $V_g = -0.5$ kV, and the gas pressure is 0.3 MPa.

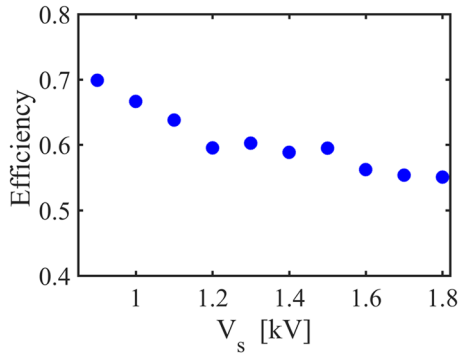


FIG. 8. Efficiency of the gun-produced arc plasma. $V_g = -0.5$ kV, and the gas pressure was 0.3 MPa.

supply to the anode of the gun. The discharging current could be limited by inserting a resistor in series, if needed, to extend the gun's lifetime. The effective resistance of the plasma is 0.037Ω .

We define the energy efficiency as the amount of stored energy converted to arc plasma energy: efficiency = $V_a I_a t_d / (1/2 \times C_n V_s^2)$, where t_d is the discharging time, ~ 1.3 ms. Figure 8 shows that the efficiency is $\sim 60\%$ in general.

III. PARAMETER SCAN

To optimize the performance of the medium-sized gun, scans were performed for various parameters, and the results are discussed in Secs. III A–III C.

A. Pressure scan

Due to its high voltage and arc current, the gun plasma is generally assumed to be fully ionized. This was confirmed in a particle inventory conducted in the GDT.¹¹ One way to raise the plasma density could be to increase the amount of injected gas flow to the gun and increase the arc voltage in accordance. However, like the gun performance reported by Fiksel *et al.*,³²

the KMAX plasma density did not exhibit a strong dependence on the injection neutral pressure.

The pressure was scanned over 0.05–0.4 MPa, with other parameters fixed. The discharge voltage was 1.5 kV, and the grid voltage was -0.5 kV. The pressure referred to the neutral pressure in the gas reservoir or at the EM valve, which was released through a 0.5-m pipe to the gun barrel when the valve opened. Plotted in Fig. 9 are traces of floating potentials and ion saturation currents collected by the A, B, and C probes located, respectively, in the east, central, and west cells. The $\sim 40\%$ increase in plasma density on probe A, which is closest to the gun, is much less than the six-fold increase in injected gas pressure (0.05–0.3 MPa). Note that neutrals diffuse more quickly at higher pressure, as shown in Fig. 4, which may have quenched the plasma and increase the recombination rate.

Fluctuations in all the probe signals are likely caused by MHD instabilities. Fortunately, they do not cause severe damage and terminate the discharge. The plasma in the central cell lasts an additional ~ 0.5 – 1.0 ms after the gun switched off, indicating good mirror confinement of the plasma. The floating potentials also change to positive values. More discussion about the after-gun plasma is in Sec. IV A.

Figure 10 plots the detailed measurements of the plasma floating potential V_f , electron temperature T_e , and plasma density n_e vs. injected gas pressure. The plasma density generally increases with the neutral pressure, while T_e remains unchanged within experimental error. The data are time-averaged values over $t = 0.8$ – 1.3 ms, with all the probes on the axis ($r = 0$ cm). The measured T_e close to the gun is only a few eV. As pointed out by Osher, who also observed $T_e \sim 5$ eV in Ref. 30, the streaming plasma was primarily the cold secondary plasma generated by energetic electrons.

B. Grid voltage scan and flow speed

A grid is widely used to extract electron or ion beams. Here, it was installed for additional plasma control at $z = 5$ m or 6 cm in front of the gun. The grid bias is applied relative to the gun anode.

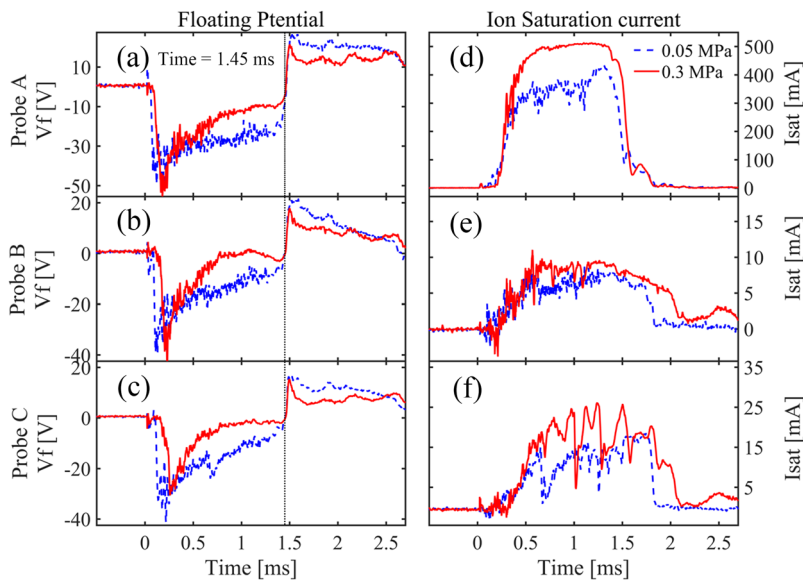


FIG. 9. Measured floating potentials and ion saturation currents at pressures of 0.05 MPa and 0.3 MPa. Probe A is in the east cell near the source, B is in the central cell, and C is in the west cell, located at $z = 3.25$ m, 0.5 m, and -3.25 m, respectively. $V_a = 1.5$ kV and $V_g = -0.5$ kV.

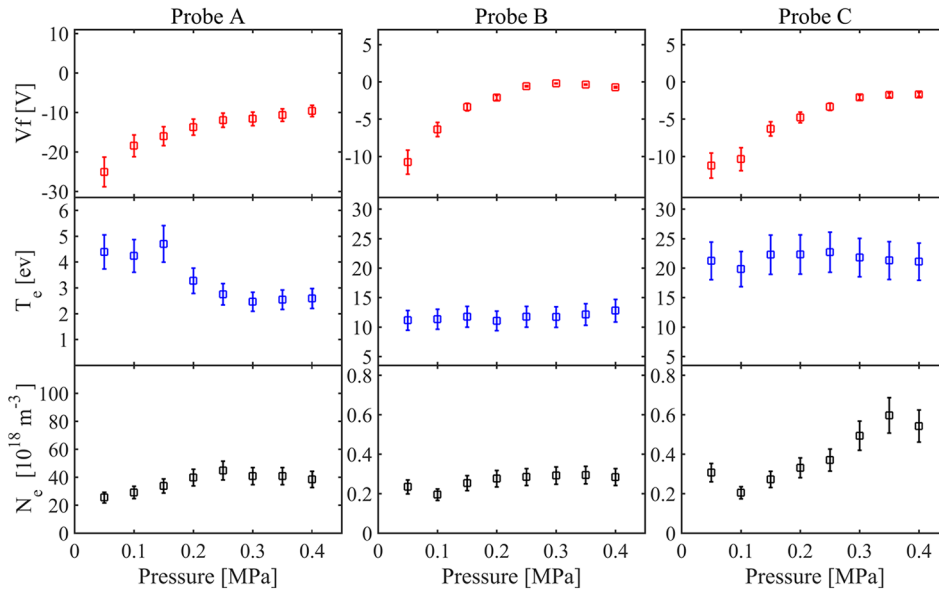


FIG. 10. Floating potential, electron temperature, and plasma density vs gas pressure at the valve. All the probes were fixed at $r = 0$ cm position. Probe A was in the east cell near the source, B was in the central cell, and C was in the west cell, located at $z = 3.25$ m, 0.5 m, and -3.25 m, respectively. $V_a = 1.5$ kV and $V_g = -0.5$ kV.

The positive grid bias results in a limited plasma in the central cell, which becomes very unstable. Thus, presented here are data taken only with the floating grid, negative bias voltages of -0.25 , -0.5 , and -0.75 kV, $V_s = 1.5$ kV, and a gas pressure of 0.3 MPa. The triple probes were scanned in a radial direction to obtain the radial plasma profiles.

Figure 11 plots the time evolution of the grid current I_g , the grid voltage relative to the gun anode V_{ga} , and the diamagnetic signal for three grid bias voltages V_g . The voltage V_{ga} is the potential difference between the grid and the anode (see the grid bias circuit in Fig. 5), while V_g is the measured grid voltage relative to ground. The bias current increases consistently with V_g . Again, after the gun is switched off at $t = 1.45$ ms, the plasma is sustained for an additional 0.1–1 ms. Those plasmas are possibly mirror-confined, as discussed

below. The remaining plasma ensures conductivity between the anode and the grid; thus, the bias power supply could be charged to negative voltage because of the PFN characteristics. The grid voltage relative to the anode V_{ga} is almost independent from V_g . The plasma pressure increases with more extracted currents, as shown in the diamagnetic measurement taken at $z = 0.3$ m. In some cases, the plasma in the central cell can be sustained for more than 2 ms after the gun switched off. It is concluded that a biased grid provides a better plasma in the central cell. The time difference labeled by red and black dashed lines in Fig. 11 is caused by the travel time from the grid location to that of the diamagnetic loop, which results in a flow speed of 30 km/s (on the order of ion sound speed).

In Fig. 12, the radial T_e , V_f , and n_e profiles are plotted for different grid voltages. The plasma radius in the central cell is ~ 15 cm, and overall, the radial electric field, calculated using dV_f/dr , is ~ 80 V/m in the east cell, ~ 25 V/m in the central cell, and ~ 30 V/m in the west cell, pointing inwards. Note that the inward electric field is essential for plasma stabilization in the C-2 device.³³

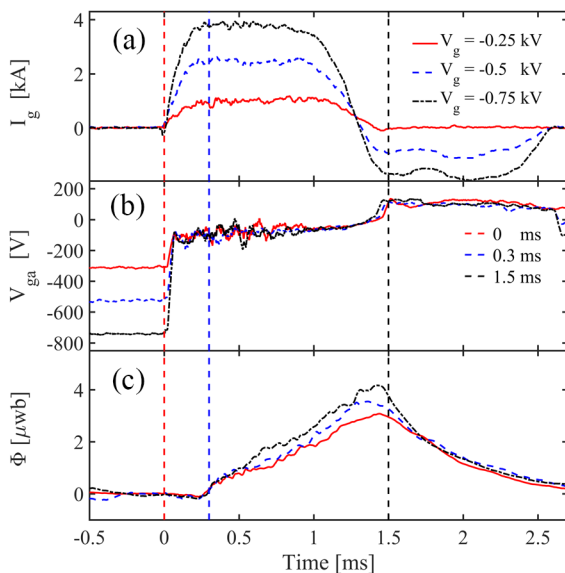


FIG. 11. (a) Traces of grid bias current, (b) voltage V_{ga} between the grid and anode, (c) and the diamagnetic signal at $z = 0.3$ cm position for $V_g = -0.25$ kV, -0.5 kV, and -0.75 kV. $V_s = 1.5$ kV, and the gas pressure is 0.3 MPa.

C. End electrode bias scan

End electrode bias has been widely used in different machines to suppress turbulence and improve confinement. Early experiments in the HIEI mirror³³ reported L- to H-mode transitions by using limiter biasing to improve radial confinement. GAMMA 10³⁴ also reported that when the potential difference between the outer mirror throat and the endplate increased, there was a significant decrease in the end loss electron flux. Another high confinement regime success was in the C-2²⁵ experiments, by edge biasing via gun-generated plasmas and neutral beams. In a GDT,³⁵ biasing limiters or peripheral endplate potentials of 250–300 V led to considerable increases in the energy confinement time.

Nevertheless, end electrode biasing in KMAX did not result in significant improvement of the plasmas (see the end electrode biasing circuit in Fig. 5). One possible reason is the

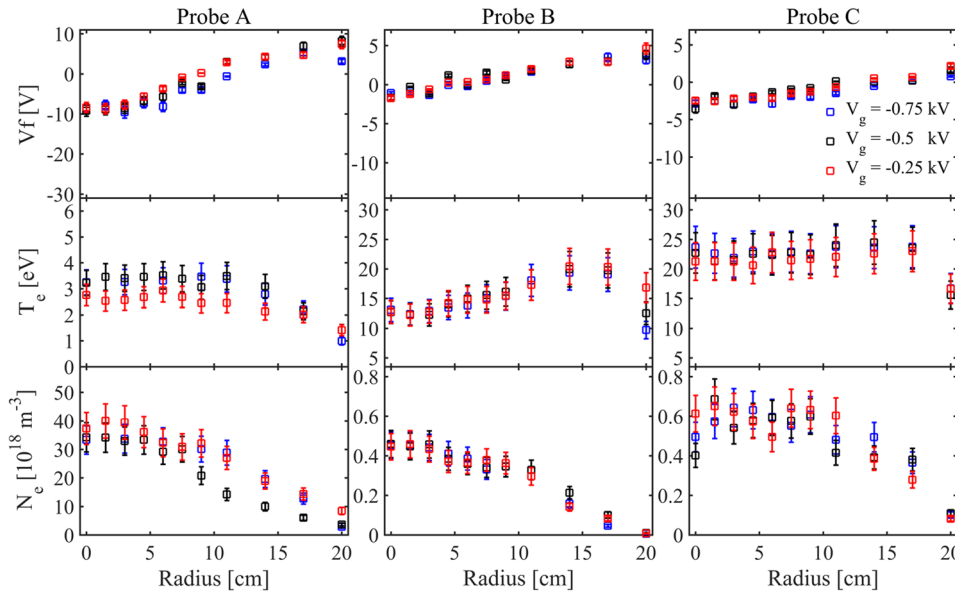


FIG. 12. Floating potentials, electron temperatures, and plasma densities vs. radius. $V_g = -0.5$ kV, and the gas pressure is 0.3 MPa. The data are averaged over the range $t = 0.8$ – 1.3 ms.

presence of MHD instabilities or other particle and energy losses that dominates the turbulence transport.

IV. DISCUSSIONS

A. Transition from gun stream to mirror confined plasma

A noticeable feature of the density evolution, especially in the central cell, is that it could last a few ms after the source/gun is switched off. In addition, the floating potential exhibits a signature jump at the gun-off time (see Fig. 9), and the transitions are indicated by dashed vertical lines. Considering the following facts:

- (1) The plasmas stream out of the gun along the pressure gradient and magnetic field direction, and the electrons lead ions out. The high-impedance probe is charged to negative potential by fast-moving electrons to retard the electrons and equalize the collected currents.³⁰
- (2) After gun is switched off, the fast axial loss of electrons leave the mirror plasma more positive.³⁶

Thus, the potential jump indicates that the plasma changes from a stream to a mirror-confined plasma after the gun is turned off.

The two different plasmas exhibit different behaviors. Initially, during the plasma buildup in the central cell, the density measurements reveal a violent process with large fluctuations in the first 1 ms [see Fig. 9(e)]. In Fig. 13, an image taken with a fast camera at $z = 0$ m shows that the plasma column is moving, where the solid line indicates the position of the plasma center. The frame rate of the fast camera is 10 kHz. Similar behavior was reported by England *et al.*³⁷ However, when the plasma transforms to the mirror-confined state, it becomes more stable, as seen after $t = 1.2$ ms in Fig. 13 and in probe B measurements for the scans discussed earlier. Figure 14 plots the normalized fluctuation levels of the two plasmas for a typical shot. Clearly, the mirror plasma is more stable after the gun is off.

B. Energy confinement of axisymmetric mirror

Established that the plasma can be categorized into two different plasmas, the energy confinement of the axisymmetric mirror could be estimated from the diamagnetic signals. We vary the east mirror ratios M to change the passage of the

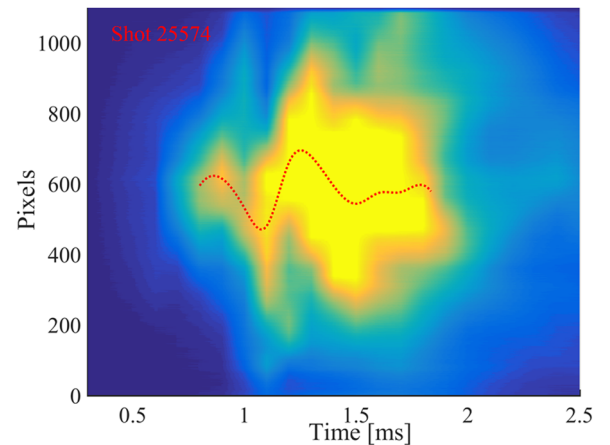


FIG. 13. Image of the plasma taken by a fast camera at $z = 0$ m. The frame rate of the fast camera is 10 kHz.

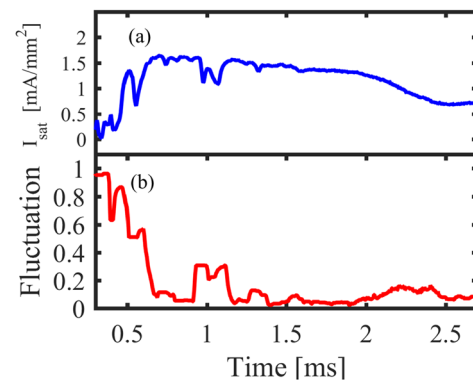


FIG. 14. (a) A typical ion saturation current collected by probe B at $z = 0.5$ m, $r = 0$ cm and (b) the normalized fluctuation level calculated from (a).

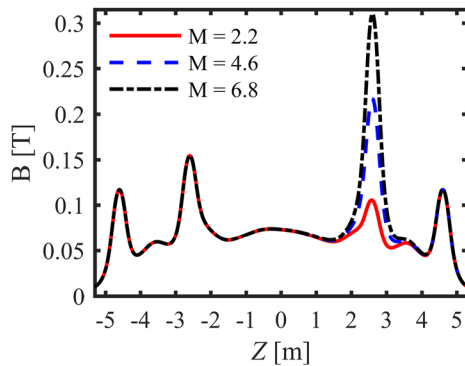


FIG. 15. Magnetic field profile for $M = 2.2$, 4.6, and 6.8.

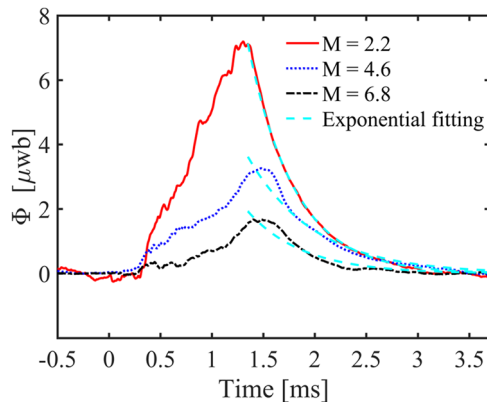


FIG. 16. Diamagnetic signal for $M = 2.2$, 4.6, and 6.8, and the diamagnetic loop at $z = 0.3$ m.

stream plasma by changing the east mirror fields. The corresponding magnetic field structure is plotted in Fig. 15 for $M = 2.2$, 4.6, and 6.8, and the diamagnetic signal measured in the central cell at $z = 0.3$ m is plotted in Fig. 16, which is consistent with the mirror effect of less plasma passing through the mirror at a higher mirror ratio.

The exponential decay during mirror confined plasma is used to estimate the energy confinement time for mirror confined plasma. For different mirror ratios presented earlier, the curve fittings of e^{-t/τ_e} yield confinement time $\tau_e \sim 0.5 \pm 0.1$ ms.

V. SUMMARY

In summary, a new medium-sized gun is developed to inject the initial plasma for the KMAX experiment, and the plasmas are investigated by varying parameters such as gas pressure, arc voltage, grid voltage, end electrode bias, and mirror fields. The typical voltage we applied is 1.5 kV with a gas pressure of 0.3 MPa. The grid is applied with negative voltage to extract more ions. However, the end electrode biasing did not result in meaningful improvement of the plasma. Though data are not shown here, we have compared a miniature gun with this medium-sized gun and found that this gun can provide more plasmas in the central cell of KMAX. Hence, it is more suitable as a plasma source for a large device. In our experiment, the plasmas undergo a transition from a stream to a mirror-confined plasma after the gun is switched off, and the

confinement time is ~ 0.5 ms. The mirror-confined plasma is more stable, as evidenced from the probe and the camera data. Future investigations will be performed on how the magnetic curvature affects the confinement or the stabilization of plasma and the detailed physics during the transition from the stream to mirror.

ACKNOWLEDGMENTS

The authors appreciate valuable discussion with Y. Feng from Soochow University. This work is supported by the National Natural Science Foundation of China (NSFC) under Grant Nos. 11475172 and 41331067, by the Key Research Program of Frontier Sciences, CAS under Grant No. QYZDJ-SSW-DQC010, and by the Chinese Academy of Sciences under Grant No. 2014.

¹D. D. Ryutov, *Sov. Phys. Usp.* **31**, 300 (1988).

²D. D. Ryutov, "Physics of mirrors, reversed field pinches and compact tori," in *Proceedings of the Course and Workshop, Varenna, Italy, 1-11 September 1987*, edited by S. Ortolani and E. Sindoni (Editrice Compositori, Bologna, 1988), pp. 791-816.

³G. I. Dimov, *Phys.-Usp.* **48**, 1129 (2005).

⁴T. K. Fowler, R. W. Moir, and T. C. Simonen, *AIP Conf. Proc.* **1771**, 080003 (2016).

⁵T. K. Fowler, R. W. Moir, and T. C. Simonen, *Nucl. Fusion* **57**, 056014 (2017).

⁶T. C. Simonen, *J. Fusion Energy* **35**, 63 (2015).

⁷G. I. Dimov and I. I. Morozov, *Rev. Sci. Instrum.* **61**, 401 (1990).

⁸S. Y. Taskaev, *Plasma Phys. Rep.* **26**, 115 (1999).

⁹A. V. Anikeev, P. A. Bagryansky, A. A. Ivanov, S. V. Kuzmin, and T. V. Salikova, *Plasma Phys. Controlled Fusion* **34**, 1185 (1992).

¹⁰A. A. Ivanov, A. V. Anikeev, P. A. Bagryansky, V. N. Bocharov, P. P. Deichuli, A. N. Karpushov, V. V. Maximov, A. A. Podminogin, A. I. Rogozin, T. V. Salikova, and Y. A. Tsidulko, *Phys. Plasmas* **1**, 1529 (1994).

¹¹P. A. Bagryansky, E. D. Bender, A. A. Ivanov, A. N. Karpushov, S. V. Murachtin, K. Noack, S. Krahl, and S. Collatz, *J. Nucl. Mater.* **265**, 124 (1999).

¹²A. A. Ivanov, A. V. Anikeev, P. A. Bagryansky, P. P. Deichuli, S. A. Korepanov, A. A. Lizunov, V. V. Maximov, S. V. Murachtin, V. Y. Savkin, D. J. Den Hartog, G. Fiksel, and K. Noack, *Phys. Rev. Lett.* **90**, 105002 (2003).

¹³M. Inutake, T. Cho, M. Ichimura, K. Ishii, A. Itakura, I. I. Katanuma, Y. Kiwamoto, Y. Kusama, A. Mase, S. Miyoshi, Y. Nakashima, T. Saito, A. Sakasai, K. Sawada, I. I. Wakaida, N. Yamaguchi, and K. Yatsu, *Phys. Rev. Lett.* **55**, 939 (1985).

¹⁴A. Mase, T. Tokuzawa, N. Oyama, Y. Ito, A. Itakura, H. Hojo, M. Ichimura, M. Inutake, and T. Tamano, *Rev. Sci. Instrum.* **66**, 821 (1995).

¹⁵S. Tanaka, M. Ichimura, S. Takayama, M. Inutake, S. Kanazawa, M. Nakamura, E. Ishikawa, C. Satake, S. Motegi, T. Saito, H. Hojo, A. Mase, K. Ishii, T. Tamano, and K. Yatsu, *Rev. Sci. Instrum.* **70**, 979 (1999).

¹⁶Y. Yoshimura, T. Saito, Y. Kiwamoto, Y. Tatematsu, T. Takahashi, K. Kajiwara, M. Kurata, M. Sakakibara, H. Abe, H. Miyaue, K. Ishii, and T. Tamano, *J. Phys. Soc. Jpn.* **65**, 902 (1996).

¹⁷Y. Morikawa, M. Yoshikawa, J. Kohagura, Y. Shima, Y. Hasegawa, M. Sakamoto, T. Imai, and M. Ichimura, *J. Instrum.* **8**, C12014 (2013).

¹⁸R. Breun, S. N. Golovato, L. Yujiri, B. McVey, A. Molvik, D. Smatlak, R. S. Post, D. K. Smith, and N. Hershkowitz, *Phys. Rev. Lett.* **47**, 1833 (1981).

¹⁹D. Sing, S. N. Golovato, N. Hershkowitz, and J. Scharer, *Phys. Fluids* **27**, 16 (1984).

²⁰G. D. Severn, N. Hershkowitz, R. A. Breun, and J. R. Ferron, *Phys. Fluids B* **3**, 114 (1991).

²¹F. H. Coensgen, C. A. Anderson, T. A. Casper, J. F. Clauser, W. C. Condit, D. L. Correll, W. F. Cummins, J. C. Davis, R. P. Drake, J. H. Foote, A. H. Futch, R. K. Goodman, D. P. Grubb, G. A. Hallock, R. S. Hornady, A. L. Hunt, B. G. Logan, R. H. Munger, W. E. Nexsen, T. C. Simonen, D. R. Slaughter, B. W. Stallard, and O. T. Strand, *Phys. Rev. Lett.* **44**, 1132 (1980).

- ²²D. L. Correll, S. L. Allen, T. A. Casper, J. F. Clauser, P. Coakley, F. H. Coensgen, W. Condit, W. F. Cummins, J. C. Davis, R. P. Drake, J. H. Foote, A. H. Futch, R. K. Goodman, D. P. Grubb, G. A. Hallock, E. B. Hooper, R. S. Hornady, A. L. Hunt, C. V. Karmendy, A. W. Molvik, W. E. Nexsen, W. L. Pickles, P. Poulsen, T. C. Simonen, B. W. Stallard, and O. T. Strand, *Nucl. Fusion* **22**, 223 (1982).
- ²³D. Craig, A. F. Almagri, J. K. Anderson, J. T. Chapman, C. S. Chiang, N. A. Crocker, D. J. DenHartog, G. Fiksel, S. C. Prager, J. S. Sarff, and M. R. Stoneking, *Phys. Rev. Lett.* **79**, 1865 (1997).
- ²⁴M. Iida, S. Masamune, and H. Oshiyama, *Jpn. J. Appl. Phys., Part 1* **39**, 1903 (2000).
- ²⁵M. Tuszewski, A. Smirnov, M. C. Thompson, S. Korepanov, T. Akhmetov, A. Ivanov, R. Voskoboynikov, L. Schmitz, D. Barnes, M. W. Binderbauer, R. Brown, D. Q. Bui, R. Clary, K. D. Conroy, B. H. Deng, S. A. Dettrick, J. D. Douglass, E. Garate, F. J. Glass, H. Gota, H. Y. Guo, D. Gupta, S. Gupta, J. S. Kinley, K. Knapp, A. Longman, M. Hollins, X. L. Li, Y. Luo, R. Mendoza, Y. Mok, A. Necas, S. Primavera, E. Ruskov, J. H. Schroeder, L. Sevier, A. Sibley, Y. Song, X. Sun, E. Trask, A. D. Van Drie, J. K. Walters, M. D. Wyman, and TAE Team, *Phys. Rev. Lett.* **108**, 255008 (2012).
- ²⁶L. Schmitz, E. Ruskov, B. H. Deng, M. Binderbauer, T. Tajima, H. Gota, M. Tuszewski, and TAE Team, *AIP Conf. Proc.* **1721**, 030002 (2016).
- ²⁷T. Matsumoto, J. Sekiguchi, T. Asai, H. Gota, E. Garate, I. Allfrey, T. Valentine, M. Morehouse, T. Roche, J. Kinley, S. Aefsky, M. Cordero, W. Waggoner, M. Binderbauer, and T. Tajima, *Rev. Sci. Instrum.* **87**, 053512 (2016).
- ²⁸M. Lin, M. Liu, G. Zhu, P. Shi, J. Zheng, Q. Lu, and X. Sun, *Rev. Sci. Instrum.* **88**, 093505 (2017).
- ²⁹C. R. Rose, in 2015 IEEE Pulsed Power Conference, Austin, TX, USA, 31 May–4 June 2015.
- ³⁰J. E. Osher, *Rev. Sci. Instrum.* **53**, 1685 (1982).
- ³¹M. J. McCarrick, R. F. Ellis, J. H. Booske, and M. Koepke, *J. Appl. Phys.* **61**, 1747 (1987).
- ³²G. Fiksel, D. Craig, M. Iida, S. C. Prager, and J. S. Sarff, *Plasma Source Sci. Technol.* **5**, 78 (1996).
- ³³O. Sakai, Y. Yasaka, and R. Itatani, *Phys. Rev. Lett.* **70**, 4071 (1993).
- ³⁴K. Kajiwara, T. Saito, Y. Kiwamoto, Y. Tatematsu, Y. Yoshimura, T. Takahashi, H. Miyaue, H. Abe, Y. Kikuchi, and T. Tamano, *J. Phys. Soc. Jpn.* **66**, 2342 (1997).
- ³⁵P. A. Bagryansky, A. A. Lizunov, A. A. Zuev, E. Y. Kolesnikov, and A. L. Solomachin, *Fusion Sci. Technol.* **43**, 152 (2003).
- ³⁶R. F. Post, *Phys. Rev. Lett.* **58**, 878 (1987).
- ³⁷A. C. England, D. K. Lee, S. G. Lee, M. Kwon, S. W. Yoon, Y. Yasaka, N. Sugimoto, I. Katanuma, K. Yashiro, and T. Imai, *Nucl. Fusion* **49**, 125008 (2009).